Japanese Journal of Applied Physics 53, 121101 (2014) REGULAR PAPER
http://dx.doi.org/10.7567/JJAP.53.121101

Oxygen flow effects on electrical properties, stability, and density of states of amorphous In–Ga–Zn–O thin-film transistors

Yong-Su Lee[1,2], Eric Kai-Hsiang Yu[2], Dong-Hwan Shim[1], Hyang-Shik Kong[1], Linsen Bie[2], and Jerzy Kanicki[2*]

[1]*Display Research Center, Samsung Display Co., Ltd., Yongin, Gyeonggi 446-711, Republic of Korea*
[2]*Solid-State Electronics Laboratory, Department of Electrical Engineering and Computer Science, University of Michigan, Ann Arbor, MI 48109, U.S.A.*
E-mail: kanicki@eecs.umich.edu

Received April 30, 2014; revised September 16, 2014; accepted October 3, 2014; published online November 12, 2014

To investigate the origin of threshold voltage (V_{th}) shift of amorphous In–Ga–Zn–O (a-IGZO) thin-film transistors (TFTs), a combination of bias-temperature stress (BTS) and multi-frequency capacitance–voltage (C–V) measurements were used to evaluate the impact of oxygen partial pressure (P_{O2}) during a-IGZO deposition on TFT electrical properties, electrical stability, and density of states (DOS). The extracted sub-gap DOS was decomposed into exponential bandtail states and Gaussian-like deep-gap states. The peak density of Gaussian-like states is larger for higher P_{O2}. We conclude that the Gaussian-like states are excess/weakly-bonded oxygen in the form of O^0 or O^{1-} ions acting as acceptor-like states and are at the origin of TFT threshold voltage shift during positive BTS. © 2014 The Japan Society of Applied Physics

1. Introduction

In the past decade, amorphous oxide semiconductors (AOS) have emerged as a promising candidate for the backplane technology of next generation ultra-high definition,[1,2] flexible,[3] and/or transparent[4] active-matrix flat-panel displays. Despite its advantages such as low processing cost and uniform deposition in the amorphous phase over a large area, AOS, especially amorphous In–Ga–Zn–O (a-IGZO), is still not yet the mainstream backplane technology in the display industry. This is primarily due to uncertainties in device processing, electrical performance including stability, and achieving a high manufacturing yield.

Different methods were proposed to improve a-IGZO thin-film transistor (TFT) electrical stability, such as thermal annealing,[5–7] hydrogen incorporation,[8] nitrogenation,[9,10] passivation,[11–13] and other methods.[14–18] However, the microscopic origin of TFT threshold voltage (V_{th}) shift is still not yet completely understood. A hypothesis proposed in the literature suggests that oxygen-related sub-band gap states, such as oxygen vacancies, are responsible for the V_{th} instability under bias-temperature stress (BTS).[19,20] To clarify the origin of V_{th} shift from an atomic-bonding point of view, X-ray photoelectron spectroscopy studies have been reported for oxygen 1s states.[7,8,21–23] Results indicated that the higher binding energy peak of oxygen 1s states is related to smaller V_{th} shift induced by BTS. It was assumed that higher oxygen flow during channel layer formation caused more oxygen being incorporated into the final a-IGZO thin film, and this was found to significantly impact device BTS stability.[24,25]

In the study of metal–oxide–semiconductor (MOS) structures, the capacitance–voltage (C–V) analysis is one of the simplest methods for probing defects. To gain insight on charge injection or defect state creation in the device during BTS of a-IGZO TFTs, C–V measurements are often performed before and after bias stressing.[26–28] Lee et al. showed that the dispersion relation of multi-frequency C–V measurements could be used to extract the a-IGZO TFT sub-gap density of states (DOS).[29] However, the relationship between device electrical stability and the sub-gap DOS was rarely studied by the C–V method. Kim et al. used the multi-frequency C–V method to compare the positive BTS (PBTS) stability and DOS of a-IGZO TFTs with channel layers sputtered in various oxygen flow ratios.[30] They found that higher oxygen flow ratio corresponded to larger PBTS-induced V_{th} shift, and that the DOS have observable differences for different flow ratios.

In this paper, we varied the oxygen flow rate during the sputtering of a-IGZO thin films and studied its impact on a-IGZO DOS and TFT electrical properties including stability under both PBTS and negative BTS (NBTS). From the TFT transfer (I_D–V_{GS}) and C–V characteristics, V_{th} and mid-gap voltage (V_{mg}) were extracted for a-IGZO TFTs before and after BTS. We extracted a-IGZO DOS from multi-frequency C–V measurements. The goal of this study is to correlate the TFT C–V and I_D–V_{GS} characteristics and parameters extracted on the same device structure. Both provide different but complementary information about the properties and stability of a-IGZO TFTs and its DOS.

2. Experiment

To fabricate bottom-gate a-IGZO TFTs, n^{++}-doped silicon wafers with 100 nm of thermal oxide (SiO_2) were used as gate electrode and gate insulator. The a-IGZO active islands (50 nm) were deposited by dc sputtering with power of 200 W at pressure of 4 mTorr under room temperature and patterned by shadow-masking. The sputtering target used has composition ratio of In : Ga : Zn : O = 2 : 2 : 1 : 7. Keeping the total gas flow into the sputtering chamber constant at 31.5 sccm, the oxygen/argon gas flow rate during IGZO sputtering was varied from $O_2/Ar = 1.5/30$, 3.2/28.3, and 4.7/26.8 sccm, which represented 5, 10, and 15% oxygen partial pressure (P_{O2}), respectively. After a-IGZO deposition, thermal annealing was performed at 350 °C for 30 min in ambient air on a hot plate. Then 100 nm of molybdenum (Mo) was sputtered as the source/drain (S/D) electrodes and also defined by shadow-masking. The fabricated common-gate TFTs were designed to have the channel width/length of 300/150 μm.

The TFT I_D–V_{GS} characteristics were measured using an Agilent B1500A semiconductor analyzer both before and after BTS at room temperature. During the measurement of the I_D–V_{GS} characteristics, the gate voltage was swept from $V_{GS} = -10$ to $+10$ V while $V_{DS} = +10$ V was applied to the drain terminal (the source terminal was grounded). The TFT

 © 2014 The Japan Society of Applied Physics

threshold voltage was extracted from the I_D–V_{GS} characteristics as the V_{GS} at which the drain current (I_D) equals 10^{-9} A. During BTS, the sample was first heated to $T_{st} = 70$ °C by a heated chuck. The Agilent B1500A then applied the gate stress voltage (V_{st}) for duration of $t_{st} = 10^4$ s while both the source and drain are grounded ($V_D = V_S = 0$ V). For PBTS tests, $V_{st} = +10$ V was applied to the TFT gate electrode, whereas $V_{st} = -10$ V was applied instead for NBTS. After BTS, the device was allowed to cool to room temperature and its I_D–V_{GS} characteristics measured again. All stressing and measurements were done in ambient air in the dark. A different device on the same wafer was used for each BTS test.

The multi-frequency TFT C–V measurements were done at room temperature before and after BTS using a HP 4284A LCR meter. The dc and the small-signal ac voltages were forced through the gate electrode, while any changes to the stored charges due to the ac signal were detected through the shorted source and drain electrodes. The frequencies of the small-signal voltage oscillations were between 20 and 500 Hz. Such low frequencies were selected to allow the charging current to arrive from the source and drain regions. At higher frequencies, the sub-gap states cannot be filled in time, and the C–V curves become flat lines with no distinct accumulation and depletion regions. This is due to the influence of the highly resistive a-IGZO bulk region.

3. Results and discussion

Figure 1 shows the C–V characteristics of the a-IGZO TFT measured at $f = 20$ Hz before and after PBTS. The C–V curve after NBTS shows no visible changes and is omitted in the figure. Only the C–V of a-IGZO channel layer sputtered in 10% O_2/Ar flow ratio is shown. Similar curves were obtained for all oxygen flow ratios studied in this work. The mid-gap voltages (V_{mg}) were extracted at the maximum inclination point in the C–V curves. Positive V_{mg} shift (ΔV_{mg}) without any change in curve slope or shape was observed after PBTS. This is also the case for TFTs with channel layers deposited at 5 and 15% oxygen flow (not shown). From these observations, we believe that the fixed and/or trapped charges near the a-IGZO/SiO_2 interface region are most likely responsible for ΔV_{mg}.[31] In this study, the fixed charges could have originated from bonding imperfections of the non-stoichiometric composition (2 : 2 : 1 : 7) a-IGZO influenced by oxygen flow changes during the deposition process. We see in Fig. 2(a) that TFTs with higher oxygen ratios have higher V_{mg}, indicating that higher oxygen flow can be responsible for larger concentration of negative oxide charges localized near or at the a-IGZO/SiO_2 interface. In Fig. 2(b), ΔV_{mg} also increased after PBTS for TFTs with higher O_2 ratios. Based on these results we can speculate that larger oxygen flow not only has impact on initial V_{mg}, but also produces larger positive shift of V_{mg} after PBTS. These effects might be due to the increase of non-stoichiometry at the a-IGZO/SiO_2 interface.

The TFT I_D–V_{GS} characteristics for different O_2/Ar ratios before and after stressing are shown in Fig. 3 for PBTS and Fig. 4 for NBTS. The device parameters extracted from the I_D–V_{GS} curves of unstressed TFTs are shown in Table I. We observe that the carrier mobility and the drain current at $V_{GS} = +10$ V (I_{on}) decreased with increasing O_2/Ar ratio. This suggests that increasing the oxygen flow rate reduced the carrier concentration of the samples tested. After stressing, the V_{th} shift (ΔV_{th}) was calculated from the difference between the V_{th} at t = 0 and 10^4 s. For PBTS, ΔV_{th} were positive for all O_2/Ar ratios, while they were all negative after NBTS. For all oxygen flow ratios studied, the extracted V_{th} and ΔV_{th} after PBTS/NBTS are shown in Figs. 5(a) and 5(b), respectively. Two observations can be made from Fig. 5: (i) ΔV_{th} is smaller for lower P_{O2} in PBTS (ii) the dependence of ΔV_{th} on P_{O2} in NBTS is insignificant. These trends are consistent with what has been reported in the literature.[30,32] For NBTS, Chen et al. showed that the ΔV_{th} of unpassivated a-IGZO TFT is strongly affected by ambient gas composition during stressing: ΔV_{th} becomes very severe when moisture is present in the ambient gas.[33] This suggests that under NBTS, ΔV_{th} is associated with the adsorption/diffusion of humidity/hydrogen/hydroxyl species in the TFT back channel. Considering that all our samples are stressed under the same ambient environment, the lack of obvious trends between NBTS and P_{O2} is within our expectations. In Fig. 6, we show that the relationship between V_{th} and V_{mg} has a linear dependence on oxygen flow ratio. From this figure, a linear relationship can be established between TFT I_D–V_{GS}

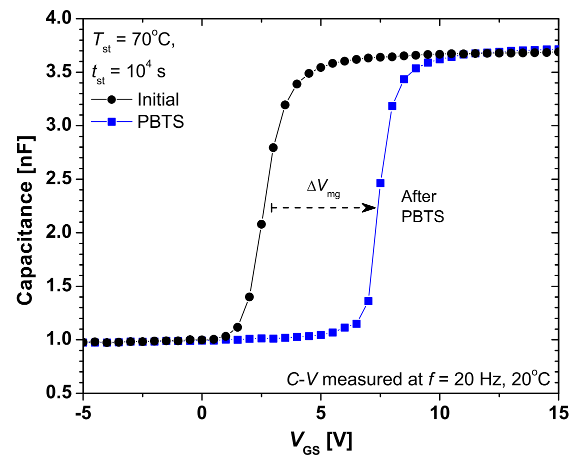

Fig. 1. (Color online) C–V curves for a-IGZO TFT with 10% O_2/Ar ratio before and after PBTS. ΔV_{mg} is the shift of mid-gap voltage before and after PBTS.

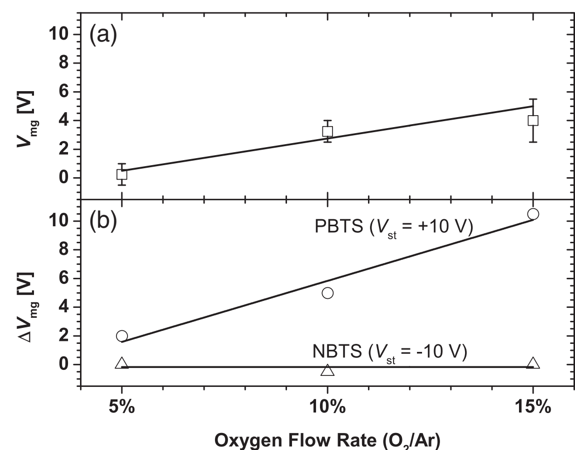

Fig. 2. (a) V_{mg} variation for different P_{O2} before BTS. (b) Shift of V_{mg} after PBTS (empty circles) and NBTS (empty triangles) for different P_{O2}. The solid lines in both sub-figures represent the linear fit to experimental data.

© 2014 The Japan Society of Applied Physics

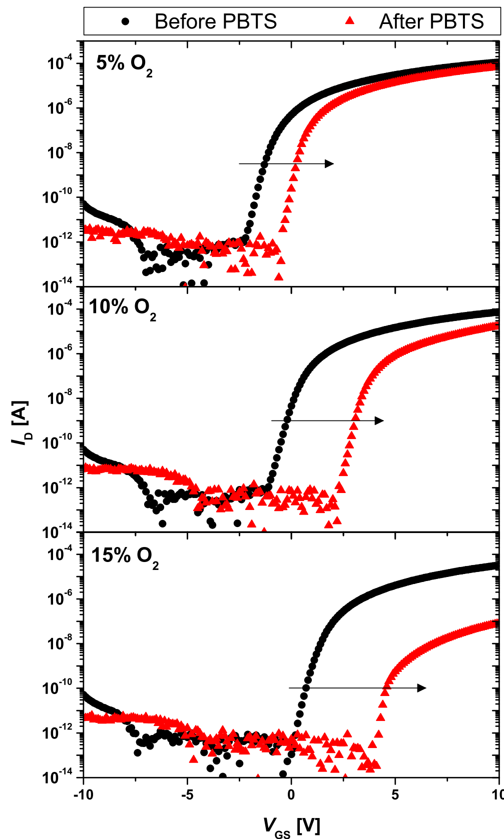

Fig. 3. (Color online) Device transfer characteristics for TFTs with different oxygen flow during sputtering. The solid circles and triangles represent before and after positive BTS ($V_{st} = +10$ V) for 10^4 s at 70 °C, respectively.

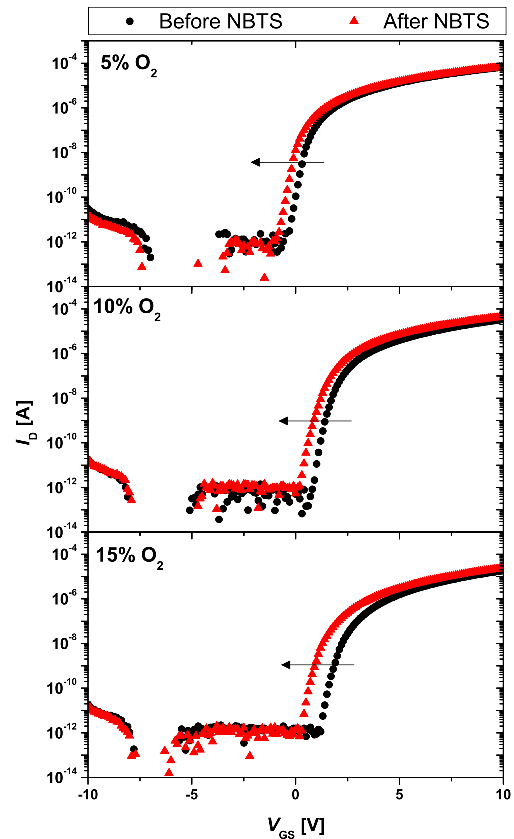

Fig. 4. (Color online) Device transfer characteristics for TFTs with different oxygen flow during sputtering. The solid circles and triangles represent before and after negative BTS ($V_{st} = -10$ V) for 10^4 s at 70 °C, respectively.

(represented by V_{th}) and C–V (represented by V_{mg}) data, which holds even after the application of PBTS. The fit parameters for the linear relationship are shown in Table II.

Measuring the C–V at different frequencies can allow us to extract the sub-gap DOS of a-IGZO[29] and investigate the influence of P_{O2}. Knowledge of a-IGZO DOS is critical for SPICE simulations and for improving the electrical properties of a-IGZO TFTs. The experimental sub-gap DOS for a-IGZO TFTs with different P_{O2} are shown in Fig. 7 as empty symbols in each sub-figure. The experimental data were extracted from multi-frequency C–V measurements following the methodology described in Ref. 29 and then fitted to the following proposed a-IGZO DOS model. The model consists of a Gaussian-like distribution and an exponential near the conduction band minimum, as given by Eqs. (1) and (2):[34,35]

$$g_G(E) = N_{ga} \exp\left[-\left(\frac{E-\lambda}{\sigma}\right)^2\right], \quad (1)$$

$$g_{exp}(E) = N_{ta} \exp\left(\frac{E-E_C}{E_a}\right). \quad (2)$$

In Eq. (1), which describes the Gaussian-like states, N_{ga}, λ and σ are the peak density, the mean energy position, and the standard deviation of the distribution, respectively. For the exponential states in Eq. (2), E_C is the conduction band edge energy, N_{ta} is the density of acceptor-like states at $E = E_C$, and E_a is the characteristic slope of the exponential states.

Table I. Initial parameters of I_D–V_{GS} curves with various O_2/Ar flow ratios during deposition.

P_{O2} (%)	I_{on} (A)	I_{off} (A)	V_{th} (V)	Mobility ($cm^2 V^{-1} s^{-1}$)	Subthreshold swing (V/dec)
5	1.14×10^{-4}	1.21×10^{-14}	−1.55	32	0.243
10	7.47×10^{-5}	2.10×10^{-14}	−0.34	27.1	0.278
15	3.21×10^{-5}	1.11×10^{-14}	1.00	16.7	0.238

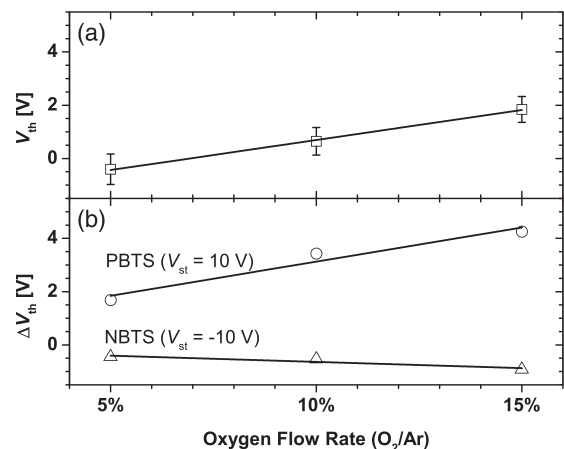

Fig. 5. (a) V_{th} variation for different P_{O2} before BTS. (b) V_{th} shift after PBTS (empty circles) and NBTS (empty triangles) for different P_{O2}. The solid lines in both sub-figures represent the linear fit to experimental data.

© 2014 The Japan Society of Applied Physics

Table II. Linear fitting curve parameters ($V_{th} = aV_{mg} + b$).

	a	b
Before PBTS	0.425	−1.36
After PBTS	0.345	−0.06

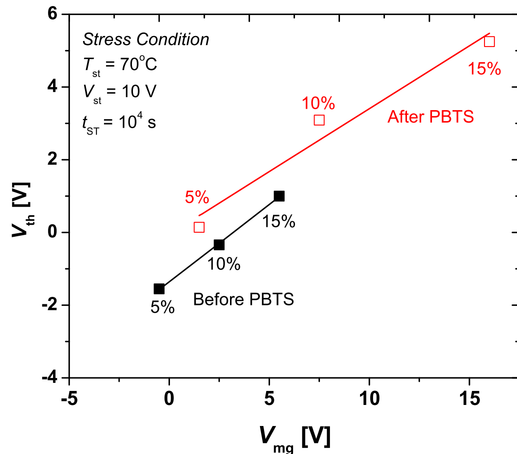

Fig. 6. (Color online) Relation between V_{th} and V_{mg} for different P_{O2} before and after PBTS.

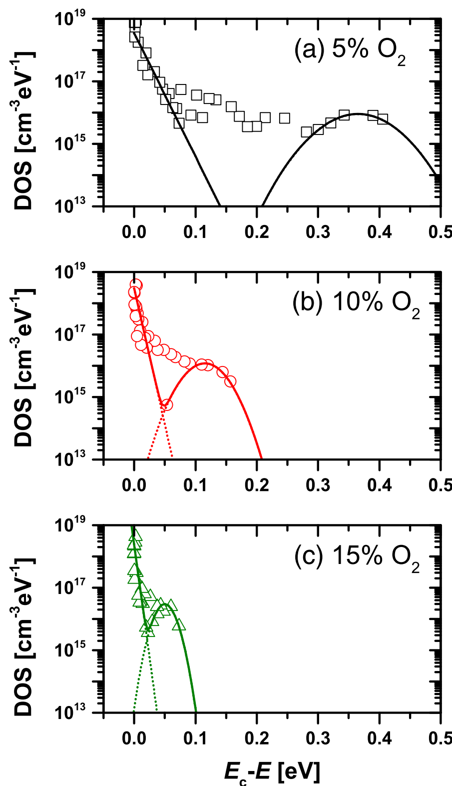

Fig. 7. (Color online) a-IGZO DOS extracted from multi-frequency C–V for P_{O2} of (a) 5, (b) 10, and (c) 15%. The solid lines are calculated from Eqs. (1) and (2), and the symbols are experimental data.

For all P_{O2} studied, the DOS fits to Eqs. (1) and (2) are shown in Fig. 7 as solid lines, and the extracted parameters of the exponential bandtail and Gaussian deep-gap DOS are shown in Tables III and IV, respectively. We note that there are minor but discernable differences in conduction bandtail states for the different P_{O2} samples: higher P_{O2} corresponded to lower N_{ta} and E_a. In a-IGZO, conduction occurs through the overlap of the large 5s orbital of the In^{3+} ion.[36] The conduction bandtail states are thus primarily a result of structural disorder, which we do not expect to be greatly affected by P_{O2}. For the a-IGZO TFTs deposited under higher P_{O2} in this study, it is possible that the lower Ar gas flow reduces the damage caused by the high-energy Ar plasma bombardment, which is reflected on the conduction bandtail states. We observe that as P_{O2} increases, the N_{ga} of the Gaussian-like deep-gap states increases and the mean energy position λ shifts towards E_C. Taking the TFT I_D–V_{GS} characteristics into consideration, increased N_{ga} directly corresponds to reduced mobility and the shift of V_{th} towards higher positive voltage. These phenomena can be explained by assuming that the deep-gap states are acceptor-like and act as electron traps. Ide et al. proposed the idea that incorporation of weakly bonded oxygen, resulting from either high-temperature O_3-annealing or high P_{O2} during a-IGZO deposition, can manifest itself as a broad distribution of deep-gap states.[37] These oxygen-related states could be either O^0 or O^{1-}, which may accept an electron to become O^{1-} or O^{2-}; O^{2-} ions could not accept an electron due to the filled outer shell. Kamiya and Hosono showed that high P_{O2} directly leads to low electrical conductivity and TFTs not entering ON-state (i.e., very high V_{th}),[38] both of which are consistent with our observations. Furthermore, the designation of these deep-gap states as acceptor-like is supported by our previous results on photoluminescence (PL) of a-IGZO thin film[34] and two-dimensional (2D) numerical simulations of a-IGZO metal-semiconductor field-effect transistors.[35] It should be noted that in Ref. 34, we concluded that the PL deep-level emission peak energy corresponds to λ of the Gaussian deep-gap states. Thus we expect the PL deep-level emission to shift towards higher energies when P_{O2} is increased. More experimental work is required to verify this hypothesis.

Table III. Exponential sub-gap DOS fitting parameters for different O_2/Ar flow rate.

P_{O2} (%)	N_{ta} ($cm^{-3}eV^{-1}$)	E_a (meV)
5	3.50×10^{18}	11
10	3.00×10^{18}	5
15	2.50×10^{18}	3

Table IV. Gaussian sub-gap DOS fitting parameters for different O_2/Ar flow rate.

P_{O2} (%)	N_{ga} ($cm^{-3}eV^{-1}$)	σ (meV)	λ (eV)
5	9.00×10^{15}	0.06	0.365
10	1.20×10^{16}	0.035	0.115
15	3.00×10^{16}	0.018	0.05

With regards to PBTS for different P_{O2}, we speculate that the larger ΔV_{th} for higher P_{O2} is also associated with the excess oxygen weakly bonded to nearest neighbors. They can exist as non-bridging or free oxygen in the a-IGZO microstructure, and their migration can be accelerated by a combination of electrical field and temperature during PBTS. If we assume that higher P_{O2} corresponds to greater incorpo-

© 2014 The Japan Society of Applied Physics

ration of excess/weakly-bonded oxygen in the a-IGZO thin film, then increased accumulation of negatively charged O^{1-} or O^{2-} ions at the a-IGZO/SiO_2 interface could reasonably account for the larger ΔV_{th} in high-P_{O2} samples. It should be noted that in Ji et al., high-pressure O_2 annealing actually reduced negative-bias illumination stress (NBIS)-induced instability.[39] This was attributed to a reduction of the oxygen vacancy (V_O^0) defects, which could be photoexcited to the V_O^{2+} charged state during NBIS and cause V_{th} to shift. Taking this into consideration along with our results on PBTS, we can then conclude that there exists a continuous spectrum of oxygen incorporation in a-IGZO, depending on deposition and annealing conditions. Oxygen-deficiency and oxygen-excess, both readily discernable through conductivity and carrier density, lead to NBIS and PBTS instability, respectively. Whether or not it is possible to optimize oxygen content for minimal PBTS and NBIS instability would require further investigation.

4. Conclusions

In this study, we found that the excess oxygen content can significantly impact a-IGZO TFT electrical characteristics. High P_{O2} reduces TFT field-effect mobility and I_{on} and increases V_{th}. When undergoing PBTS ($V_{st} = +10$ V), higher P_{O2} corresponds to larger ΔV_{th}, while no clearly discernable trend is observed for NBTS. The sub-gap DOS of a-IGZO are decomposed into exponential bandtail states and Gaussian-like deep-gap states, according to the DOS model we have adopted. The peak density of the Gaussian-like distributions is larger for higher P_{O2} during deposition. Assuming that high P_{O2} during deposition is associated with incorporation of excess/weakly-bonded oxygen in the a-IGZO thin film, then we can conclude that these deep-gap states are acceptor-like electron trap states in the form of O^0 or O^{1-} ions. The O^0/O^{1-} ions may trap an electron and become O^{1-}/O^{2-}, reducing free carriers and increasing V_{th}. During PBTS, the migration of these ion species can be accelerated by a combination of electric field and temperature, and increased accumulation at the a-IGZO/SiO_2 interface causes ΔV_{th} to become more severe.

Acknowledgment

This research was supported by Samsung Display Co., Ltd. under the Visiting Scholar Program 2013.

1) N. Gong, C. Park, J. Lee, I. Jeong, H. Han, J. Hwang, J. Park, K. Park, H. Jeong, Y. Ha, and Y. Hwang, SID Symp. Dig. Tech. Pap. **43**, 784 (2012).
2) Y. Matsueda, Dig. Int. Thin-Film Transistor Conf., 2010, p. 314.
3) H. Yamaguchi, T. Ueda, K. Miura, N. Saito, S. Nakano, T. Sakano, K. Sugi, I. Amemiya, M. Hiramatsu, and A. Ishida, SID Symp. Dig. Tech. Pap. **43**, 1002 (2012).
4) H.-H. Hsieh, T.-T. Tsai, C.-M. Hu, C.-L. Chou, S.-F. Hsu, Y.-C. Wu, C.-S. Chuang, L.-H. Chang, and Y. Lin, SID Symp. Dig. Tech. Pap. **42**, 714 (2011).
5) K. Nomura, T. Kamiya, H. Ohta, M. Hirano, and H. Hosono, Appl. Phys. Lett. **93**, 192107 (2008).
6) K. Ide, Y. Kikuchi, K. Nomura, T. Kamiya, and H. Hosono, Thin Solid Films **520**, 3787 (2012).
7) C.-S. Fuh, P.-T. Liu, Y.-T. Chou, L.-F. Teng, and S. M. Sze, ECS J. Solid State Sci. Technol. **2**, Q1 (2013).
8) S. W. Tsao, T. C. Chang, S. Y. Huang, M. C. Chen, S. C. Chen, C. T. Tsai, Y. J. Kuo, Y. C. Chen, and W. C. Wu, Solid-State Electron. **54**, 1497 (2010).
9) P.-T. Liu, Y.-T. Chou, L.-F. Teng, F.-H. Li, and H.-P. Shieh, Appl. Phys. Lett. **98**, 052102 (2011).
10) J. Raja, K. Jang, N. Balaji, W. Choi, T. T. Trinh, and J. Yi, Appl. Phys. Lett. **102**, 083505 (2013).
11) K. Nomura, T. Kamiya, and H. Hosono, Thin Solid Films **520**, 3778 (2012).
12) W.-T. Chen, S.-Y. Lo, S.-C. Kao, H.-W. Zan, C.-C. Tsai, J.-H. Lin, C.-H. Fang, and C.-C. Lee, IEEE Electron Device Lett. **32**, 1552 (2011).
13) S.-H. K. Park, M.-K. Ryu, H. Oh, C.-S. Hwang, J.-H. Jeon, and S.-M. Yoon, J. Vac. Sci. Technol. B **31**, 020601 (2013).
14) G. Baek, K. Abe, A. Kuo, H. Kumomi, and J. Kanicki, IEEE Trans. Electron Devices **58**, 4344 (2011).
15) H.-W. Zan, W.-T. Chen, C.-W. Chou, C.-C. Tsai, C.-N. Huang, and H.-W. Hsueh, Electrochem. Solid-State Lett. **13**, H144 (2010).
16) X. Huang, C. Wu, H. Lu, F. Ren, D. Chen, R. Zhang, and Y. Zheng, Appl. Phys. Lett. **102**, 193505 (2013).
17) S. Yasuno, T. Kita, A. Hino, S. Morita, K. Hayashi, and T. Kugimiya, Jpn. J. Appl. Phys. **52**, 03BA01 (2013).
18) B. S. Park, D. K. Yim, S.-M Cho, S. Y. Choi, and J. M. White, ECS Trans. **54** [1], 97 (2013).
19) H.-K. Noh, K. J. Chang, B. Ryu, and W.-J. Lee, Phys. Rev. B **84**, 115205 (2011).
20) B. Ryu, H.-K. Noh, E.-A. Choi, and K. J. Chang, Appl. Phys. Lett. **97**, 022108 (2010).
21) K. Nomura, T. Kamiya, E. Ikenaga, H. Yanagi, and K. Kobayashi, J. Appl. Phys. **109**, 073726 (2011).
22) B. Kim, E. Chong, D. Kim, Y. Jeon, D. Kim, and S. Lee, Appl. Phys. Lett. **99**, 062108 (2011).
23) T. Trinh, V. Nguyen, K. Ryu, K. Jang, W. Lee, S. Baek, J. Raja, and J. Yi, Semicond. Sci. Technol. **26**, 085012 (2011).
24) H.-H. Hsieh, C.-H. Wu, C.-W. Chien, C.-K. Chen, C.-S. Yang, and C.-C. Wu, J. Soc. Inf. Disp. **18**, 796 (2010).
25) X. Xiao, W. Deng, S. Chi, Y. Shao, X. He, L. Wang, and S. Zhang, IEEE Trans. Electron Devices **60**, 4159 (2013).
26) C.-Y. Jeong, D. Lee, S.-H. Song, J. I. Kim, J.-H. Lee, and H.-I. Kwon, Semicond. Sci. Technol. **29**, 045023 (2014).
27) Y. Kim, S. Kim, W. Kim, M. Bae, H. K. Jeong, D. Kong, S. Choi, D. M. Kim, and D. H. Kim, IEEE Trans. Electron Devices **59**, 2699 (2012).
28) S.-H. Choi and M.-K. Han, Appl. Phys. Lett. **100**, 043503 (2012).
29) S. Lee, S. Park, S. Kim, Y. Jeon, K. Jeon, J.-H. Park, J. Park, I. Song, C. Kim, Y. Park, D. Kim, and D. H. Kim, IEEE Electron Device Lett. **31**, 231 (2010).
30) S. Kim, Y. W. Jeon, Y. Kim, D. Kong, H. K. Jung, M.-K. Bae, J.-H. Lee, B. D. Ahn, S. Y. Park, J.-H. Park, J. Park, H.-I. Kwon, D. M. Kim, and D. H. Kim, IEEE Electron Device Lett. **33**, 62 (2012).
31) S. M. Sze and K. K. Ng, *Physics of Semiconductor Devices* (Wiley, New York, 2007) 3rd ed., p. 197.
32) W.-T. Chen, S.-Y. Lo, S.-C. Ko, H.-W. Zan, C.-C. Tsai, J.-H. Lin, C.-H. Fang, and C.-C. Lee, IEEE Electron Device Lett. **32**, 1552 (2011).
33) Y.-C. Chen, T.-C. Chang, H.-W. Li, S.-C. Chen, W.-F. Chung, Y.-H. Chen, Y.-H. Tai, T.-Y. Tseng, and F.-S. Yeh(Huang), Thin Solid Films **520**, 1432 (2011).
34) C. Zhao, L. Bie, R. Zhang, and J. Kanicki, IEEE Electron Device Lett. **35**, 75 (2014).
35) E. K.-H. Yu, S. Jun, D. H. Kim, and J. Kanicki, J. Appl. Phys. **116**, 154505 (2014).
36) T. Kamiya, K. Nomura, and H. Hosono, J. Disp. Technol. **5**, 468 (2009).
37) K. Ide, Y. Kikuchi, K. Nomura, M. Kimura, T. Kamiya, and H. Hosono, Appl. Phys. Lett. **99**, 093507 (2011).
38) T. Kamiya and H. Hosono, ECS Trans. **54** [1], 103 (2013).
39) K. H. Ji, J.-I. Kim, H. Y. Jung, S. Y. Park, R. Choi, U. K. Kim, C. S. Hwang, D. Lee, H. Hwang, and J. K. Jeong, Appl. Phys. Lett. **98**, 103509 (2011).

© 2014 The Japan Society of Applied Physics